Available online at www.sciencedirect.com
ScienceDirect
Journal of the European Ceramic Society 29 (2009) 1947–1954
www.elsevier.com/locate/jeurceramsoc

Compressibility and sinterability of CeO_2–8YSZ powders synthesized by a wet chemical method

A.A. Bukaemskiy, D. Barrier, G. Modolo *

Institute for Energy Research, Safety Research and Reactor Technology, Forschungszentrum Jülich GmbH, D-52425 Jülich, Germany

Received 11 July 2008; received in revised form 21 November 2008; accepted 3 December 2008
Available online 20 January 2009

Abstract

The compressibility and sinterability of CeO_2–8YSZ powders prepared by co-precipitation were investigated in detail. It was shown that the compressibility curves are characterized by three linear parts at low, middle and high pressures. The middle and high regions of the applied pressure, as least investigated, were studied in detail. The specific values of the compaction pressure (P_{Y2}) and density (ρ_{Y2}) at the intersection point of the compressibility curves were determined for all investigated powders. It was shown that the compressibility curves for all investigated powders can be described by two straight lines by using special coordinates ρ_G/ρ_{Y2} and $\log(P/P_{Y2})$.

The sinterability curves of powders after drying and after calcination at 350 °C have a pronounced maximum. The optimum compaction pressures (P^*) corresponding to the pressure at the maximal value of sintered density were determined for all investigated powders. It was shown that the region of optimal pressures is in the upper part of the middle-pressure region, whereas the P^*/P_{Y2} ratio varies between 0.7 and 0.9. The influence of the powder fractionation on the sinterability of the powders was also studied in detail as a function of the compaction pressure and calcination temperature.

Keywords: Pressing; Sintering; Microstructure; ZrO_2; Nuclear applications

1. Introduction

Zirconia-based materials have been successfully used in many areas of science and technology, including the nuclear engineering. In recent years, cubic yttria stabilized zirconia (YSZ) has been considered one of the most promising matrices for the immobilisation of plutonium and minor actinides (Am, Cm, Np), as a stable host phase for long-term final disposal, as well as a fuel/target material for transmutation.[1–3] According to Ref. [4], yttria cubic stabilized ZrO_2 is the most appropriate material in comparison with other possible alternatives, since it satisfies the criteria for an inert matrix, such as phase stability over a large temperature range and under severe irradiation; inertness with regard to transmutation products, cladding, and reactor water; small thermal neutron adsorption cross-section, etc. Moreover, this material has the ability to form solid solutions over a wide range of solubility with compounds such as UO_2, ThO_2, and PuO_2 and with rare-earth trivalent oxides.[5]

In experimental investigations, cerium is traditionally used as a surrogate of tetravalent actinides, for example, plutonium.[2,5,6] Cerium and plutonium have almost identical ionic radii, and the lattice parameters for PuO_2 and for CeO_2 are very similar.[7,8]

For nuclear applications, the technological cycle of ceramic production should be dust-free and use low-cost starting materials and an easy fabrication process.[9] Therefore, in this case, many traditional powder technologies are either inefficient or must be specially adapted. The co-precipitation method used in this work is sufficiently simple, dust-free powder technology, which is suitable for nuclear applications.[9] Furthermore, for the powder preparation for sintering, technological operations such as dry milling and high-temperature calcination are undesirable. Therefore, synthesized powders were prepared by calcination at low temperatures (up to 800 °C) and mild attrition grinding in liquid. A careful study of the processes occurring during of the compacting and subsequent sintering powders is essential for the production of a ceramic with the required properties.

* Corresponding author. Tel.: +49 2461 614896; fax: +49 2461 612450.
E-mail address: g.modolo@fz-juelich.de (G. Modolo).

0955-2219/$ – see front matter © 2008 Elsevier Ltd. All rights reserved.
doi:10.1016/j.jeurceramsoc.2008.12.005

In the present work, the compressibility and sinterability of CeO_2–8YSZ powders prepared by the co-precipitation method were investigated in detail. Moreover, the influence of the powder fractionation on the sinterability of the powders was also studied in detail as a function of the compaction pressure and calcination temperature.

2. Experimental

CeO_2–8YSZ powders with 8 and 12 mol% ceria were synthesized by the co-precipitation method. For all powders, the concentration of Y_2O_3 in the zirconia matrix was kept constant at 8 mol%.

$ZrOCl_2{\cdot}6H_2O$ (Alfa Aesar, 99.9%.), $Y(NO_3)_3{\cdot}6H_2O$ (Alfa Aesar, 99.9%.) and $Ce(NO_3)_3{\cdot}6H_2O$ (Alfa Aesar, 99.9%) were used as initial materials. The required quantity of the salts was dissolved in deionised water at room temperature, reaching a concentration of $\sim 10^{-2}$ mol/L. For the co-precipitation, ammonia gas was added to the surface of the solution and stirred for 30 min in order to ensure a homogeneous reaction. Precipitates were washed using the Büchner system until the pH of the solution became neutral.

After washing, the both powders were dried in a furnace at 110 °C for 24 h. The $8CeO_2$–8YSZ powder was then calcined in air at 350, 600 and 800 °C for 2 h. After calcination, the powders were attrition ground for 2 h in acetone to prevent dust formation. The $12CeO_2$–8YSZ powder was investigated only after drying.

The powders (approximately 0.5 g) were compacted into cylindrical pellets of 10 mm diameter by cold uniaxial pressing. The range of pressures used for this work varied from 25 to 1020 MPa.

The pellets were sintered at 1600 °C for 5 h in air atmosphere in an electric resistance furnace (Linn HT 1800).

The morphological structures of green bodies were investigated using a scanning electron microscope (SEM), (JEOL JSM-840). Particle size distribution was studied by optical microscopy (Zeiss KS300) and laser granulometry (Quantachrom, Cilas 920).

Sintered pellets were carefully polished with diamond paste (1 μm) for further investigations of the microstructure. For SEM investigations, the samples were thermally etched in air at 1400 °C for 1 h and then their morphology was analysed.

The densities of the green bodies were measured by the geometrical method, the densities of the sintered bodies by hydrostatic weighing in water.

3. Results and discussion

After synthesis and drying, both $8CeO_2$–8YSZ and $12CeO_2$–8YSZ powders contained agglomerates with irregular shapes, which differed in their primary particles packing density, as shown in Fig. 1a for the representative case of $8CeO_2$–8YSZ powder. According to the literature,[10,11] the agglomerates with a high-packed density of primary particles are referred to as "hard" agglomerates (Fig. 1b), while the low-packed agglomerates are "soft" agglomerates (Fig. 1c).

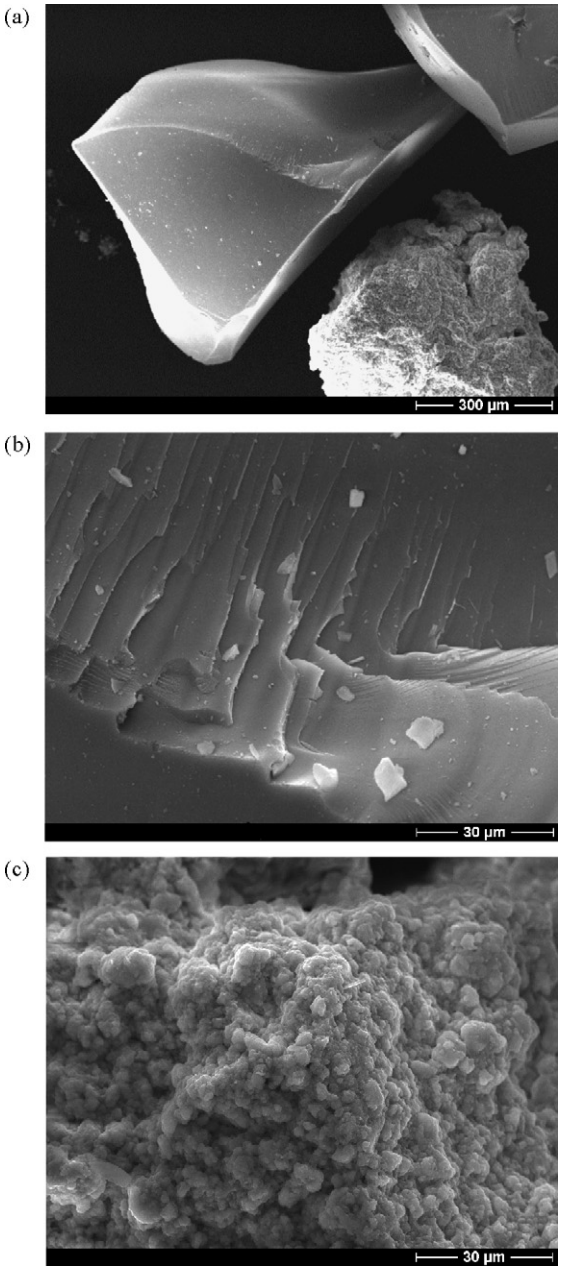

Fig. 1. SEM image of (a) 8YSZ–CeO_2 powder after drying, (b) "hard" and (c) "soft" agglomerates.

After calcination at 110, 350, 600 and 800 °C, the powders were mildly attrition ground in acetone and the agglomerate size distribution was investigated using an optical microscope. For the representative case of the $8CeO_2$–8YSZ powder calcined at 600 °C, the mass distribution is shown in Fig. 2a. The agglomerate size distribution up to 60 μm features two maxima at 12 and 48 μm.

The fine fraction of the powders was separated by sedimentation method[12,13] using acetone as the sedimentation liquid. For all investigated powders, the suspension of the fine fraction was separated at the similar experimental conditions (initial concentration of powder in liquid, settling time, etc.), then the acetone was evaporated, and amount of the fine fraction was determined.

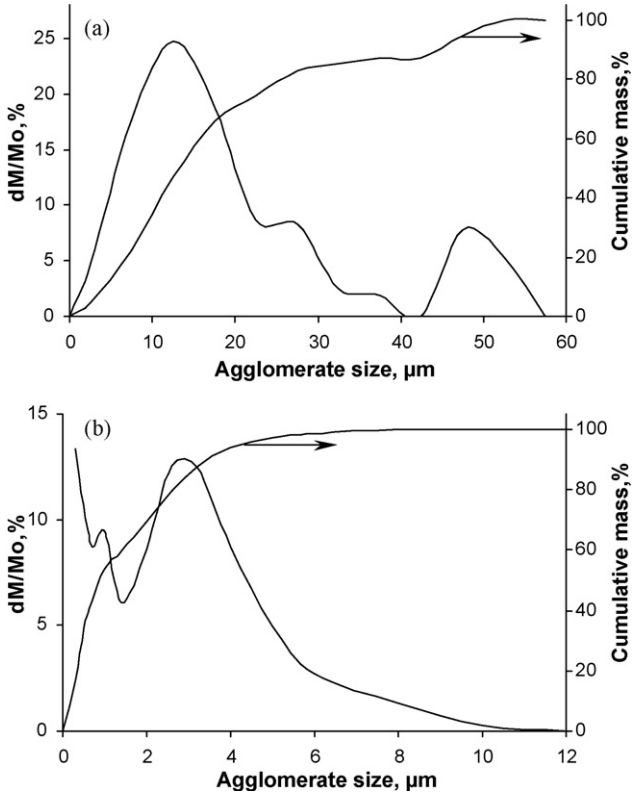

Fig. 2. Agglomerate size and cumulative mass distributions for $8CeO_2$–8YSZ powder (a) after attrition grinding and (b) after fractionation.

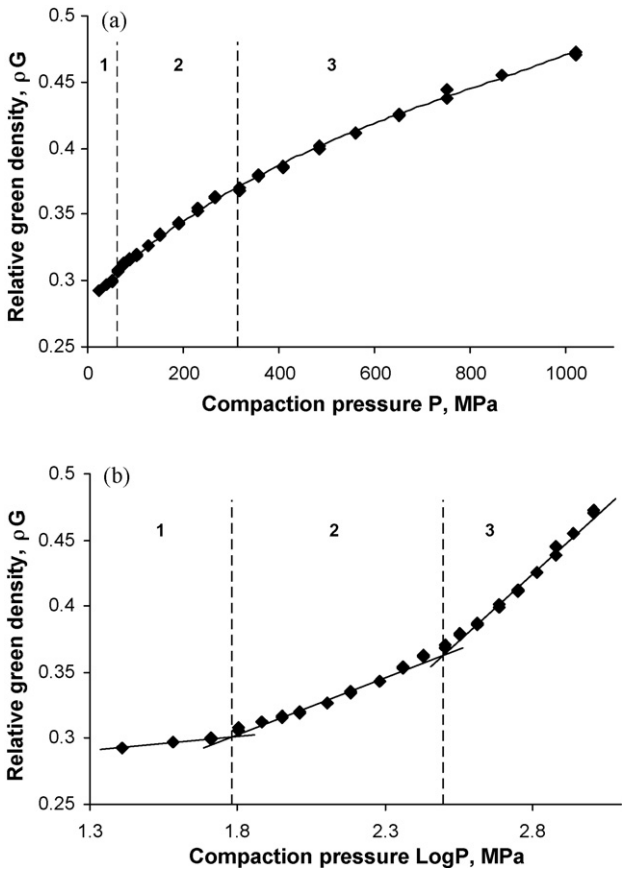

Fig. 3. Relative green densities (ρ_G) of $12CeO_2$–8YSZ powder after drying as function of (a) compaction pressure (P) and (b) log P.

For example, for the powders calcined at 110, 600 and 800 °C, this value is about 66, 40 and 8%, respectively. It was shown that the fine fraction consists of both types of agglomerates, while the coarse fraction consists mainly of the "hard" agglomerates. The mass distribution for the fine fraction determined by the laser granulometry is shown in Fig. 2b for the representative case of the $8CeO_2$–8YSZ powder calcined at 600 °C. The agglomerate size distribution has a well-defined maximum at 2.7 μm, whereas about 95 wt.% of the agglomerates have an equivalent diameter of less than 4 μm, and the average agglomerate size is equal to 0.9 μm.

3.1. Compressibility of the powders

The investigated powders were compacted by cold uniaxial pressing, applying pressures between 25 and 1020 MPa. For the $12CeO_2$–8YSZ powder after drying, the values of the relative green densities (ρ_G) were plotted as a function of the compaction pressure (P) and, as recommended in Refs. [14,15], as a function of log P (Fig. 3).

The compressibility curves are characterized by three linear regions at low, middle and high pressures with intersection points at $P_{Y1} = 81$ MPa and $\rho_{Y1} = 0.31$ and at $P_{Y2} = 310$ MPa and $\rho_{Y2} = 0.36$ (Fig. 3a). Each linear region can be described by an empirical equation[15]:

$$\rho_G = A_i \ \log \ P + B_i \quad (1)$$

where A_i, B_i are empirical constants for the low ($i = 1$), middle ($i = 2$) and high ($i = 3$) pressure regions, respectively.

The compaction behaviour of the ceramic powders in the regions of low and middle pressures was studied in detail in Refs. [15–17]. For the cubic yttria stabilized zirconia (8.5YSZ) powders synthesized by wet chemical methods (gel-precipitation) in Ref. [17], the compressibility curve consists of two linear regions with a single intersection point at pressure $P_{Y1} = 30$ MPa and $\rho_{Y2} = 0.2$. The process of powder compaction was considered on the basis of the microstructural development during compression. It was shown that the powders synthesized by the wet chemical method are built up from three microstructural elements: (1) primary crystallites, (2) crystallites densely packed into small and strong aggregates, and (3) weak and highly porous agglomerates consisting of the aggregates. The authors demonstrated that at pressures below P_{Y1}, the agglomerates are only rearranged and partially fragmentised without a change in their internal microstructure. At the pressure around and higher than P_{Y1}, compression of the agglomerates occurs, which causes changes in their internal microstructure.

The value of P_{Y1} is the average compression strength of the agglomerates and it depends heavily on the method of synthesis.[17] The empirical constant A_2 is related to the microstructure of the powder and increases with increasing hardness of the agglomerates.[17]

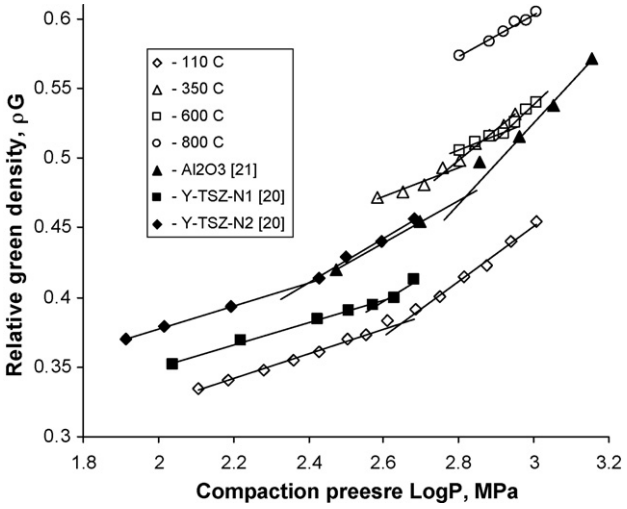

Fig. 4. Compressibility curves for $8CeO_2$–8YSZ powders calcined at different temperature, and reference data.

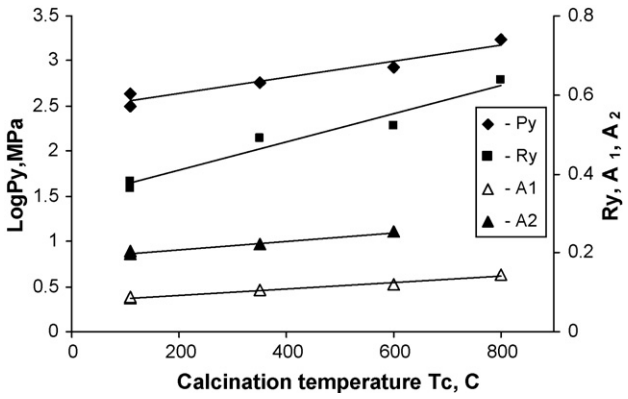

Fig. 5. Dependencies of $\log P_{Y2}$, ρ_{Y2}, A_1 and A_2 on calcination temperature T_C for $8CeO_2$–8YSZ powder.

The compressibility of the ceramic powders in the high-pressure region (around the second breakpoint $\rho_{Y2} - P_{Y2}$) has mainly been investigated in detail for spray-dried powders.[18–21] The compressibility curves of these powders are also characterized by the presence of two breakpoints. The pressure at the second breakpoint (P_{Y2}) denoted as "joining pressure" corresponds to the powder condition where the granules (or the agglomerates) lose their separate identity. At this stage, the compact behaviour is similar to the same non-granulated (agglomerated) powder, i.e. only a rearrangement of the crystallites takes place.[16] However, as described in Refs. [19,18], the mechanistic interpretation of this slope change is complex and uncertain. It may be also interpreted as an artefact of the elastic compression of the compact and/or the elastic response of the testing fixture. Moreover, unlike wet synthesized powders, for some spray-dried powders, the slope of the compressibility curves in the high-pressure region is smaller than that in the middle-pressure region. This is apparently due to a peculiar morphology of the spray-dried powders.[20,21]

There are insufficient studies on the compressibility of the powders synthesized by wet chemical methods.[22,23] On the basis of the experimental results in Ref. [22], for the (Y-TZP) powders after calcination at 450 °C, it is possible to suppose the presence of a second break point in the compressibility curves at $P_{Y2} \sim 200$–400 MPa and $\rho_{Y2} \sim 0.3$–0.4 (Fig. 4). Li and Ye studied[23] the compressibility curve for the alfa-Al_2O_3 nanopowder synthesized by the polyacrylamide gel method and calcined at 1000 °C in the range of compression pressures between 300 and 1480 MPa. They found a breakpoint at $P_{Y2} \sim 700$ MPa and $\rho_{Y2} \sim 0.47$ (Fig. 4). However, both studies lack a physical interpretation and detailed investigations of the second breakpoint in the compressibility curves. Therefore, in the present work, the middle and high regions of the applied pressure were studied in detail.

The compressibility curves for the investigated powders together with reference data are shown in Fig. 4. For the powders calcined at temperatures below 800 °C, a second break was found in the compressibility curves (Fig. 4). The values of P_{Y2}, ρ_{Y2}, A_i and B_i are shown in Table 1. From Table 1, it is obvious that the strength of the microstructural components (P_{Y2}), their characteristic packing density (ρ_{Y2}) and the values of A_2 and A_3 increase with increasing calcination temperature T_C. In all cases, the dependencies of these characteristics on T_C are linear (Fig. 5).

Eq. (1) for both regions of the compressibility curve after normalization with respect to P_{Y2} and ρ_{Y2} can be rewritten as:

$$\frac{\rho_G}{\rho_{Y2}} = 1 + \frac{A_2}{\rho_{Y2}} \log\left(\frac{P}{P_{Y2}}\right) \quad \text{for} \quad P < P_{Y2} \tag{2}$$

Table 1
Characteristics of compressibility curves.

Material	Synthesis	T_C (°C)	ρ_{Y2} (g/sm^3)	P_{Y2} (MPa)	A_2	B_2	A_3	B_3	A_3/A_2
$12CeO_2$–8YSZ	Co-precipitation and H_2O	110	0.36	309	0.086	0.149	0.203	−0.143	2.37
$8CeO_2$–8YSZ	Co-precipitation and H_2O	110	0.38	439	0.088	0.147	0.197	−0.139	2.23
$8CeO_2$–8YSZ	Co-precipitation and H_2O	350	0.49	573	0.105	0.199	0.221	−0.120	2.10
$8CeO_2$–8YSZ	Co-precipitation and H_2O	600	0.52	858	0.121	0.168	0.253	−0.221	2.10
$8CeO_2$–8YSZ	Co-precipitation and H_2O	800	0.64[a]	1720[a]	0.146	0.165			
Y-TZP[20] N1	Co-precipitation and H_2O	450	0.40	392	0.075	0.203	0.163	−0.027	2.19
Y-TZP[20] N2	Co-precipitation and 97%H_2O + 3%oil	450	0.40	199	0.075	0.226	0.123	0.115	1.64
Y-TZP[20] N3	Co-precipitation and 3.5%H_2O + 96.5%C_2H_5OH	450	0.40	249	0.061	0.253	0.107	0.142	1.76
Y-TZP[20] N4	Co-precipitation and 10%H_2O + 90%C_3H_7OH	450	0.33	211	0.140	0.009	0.206	−0.144	1.47
Al_2O_3[21]	Polyacrylamide gel method and calcination	1000	0.47	671	0.152	0.045	0.295	−0.361	1.95

[a] Calculated value.

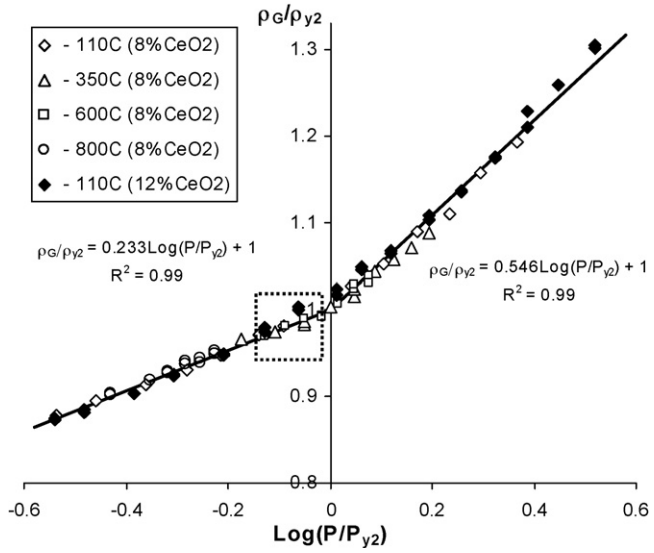

Fig. 6. Compressibility curve for all investigated powders in coordinates ρ/ρ_{Y2} and $\log(P/P_{Y2})$.

$$\frac{\rho_G}{\rho_{Y2}} = 1 + \frac{A_3}{\rho_{Y2}} \log\left(\frac{P}{P_{Y2}}\right) \quad \text{for} \quad P > P_{Y2} \tag{3}$$

The compressibility curves for the $8CeO_2$–8YSZ powders after calcination at 110, 350, 600 °C and for the $12CeO_2$–8YSZ powder after drying in coordinates ρ/ρ_{Y2} and $\log(P/P_{Y2})$ are shown in Fig. 6.

From this figure is obvious that all of our experimental data is described by two straight lines (the correlation factor $R_2 \sim 0.99$), and that the empirical coefficients A_2/ρ_{Y2} and A_3/ρ_{Y2} are constant and equal 0.23 and 0.56, respectively. Moreover, in contrast to A_2 and A_3, these values are independent of the powder composition (8 or 12 mol% CeO_2) and calcination temperature T_C. As a result, these parameters are universal characteristics of powder compressibility.

In the case of the powder after calcination at 800 °C, the compressibility curve can be described by one straight line. However, it is logical to suppose that the corresponding value of P_{Y2} is higher than the maximum pressure used in our experiments, i.e. $P_{Y2} > 1020$ MPa. The values of P_{Y2} and ρ_{Y2} for this powder can be estimated from Eq. (2). From the values of A_2, B_2 and the relation $A_2/\rho_{Y2} = 0.233$, ρ_{Y2} equals 0.64 and $\log(P_{Y2}) = (\rho_{Y2} - B_2)/A_2 = 3.24$ or $P_{Y2} = 1720$ MPa. Taking into account the obtained values, the compressibility curve for powder calcined at 800 °C was recalculated and is shown in Fig. 6.

Apparently, the compressibility of the powders is determined mainly by the conditions of powder synthesis and by subsequent treatment. Thus, for the powders synthesized by other wet chemical methods,[22,23] the values of P_{Y2}, ρ_{Y2}, A_i and B_i determined from the reference experimental data differ significantly from our results (Table 1). Depending on the method of synthesis, washing, and calcination, the slope of the compressibility curve (A_i/ρ_{Y2}) changes from 0.15 to 0.42 for the middle-pressure region, and from 0.27 to 0.62 at high pressures. For comparison, for all of our powders, the values of A_2/ρ_{Y2} and A_3/ρ_{Y2} equal 0.23 and 0.56, respectively.

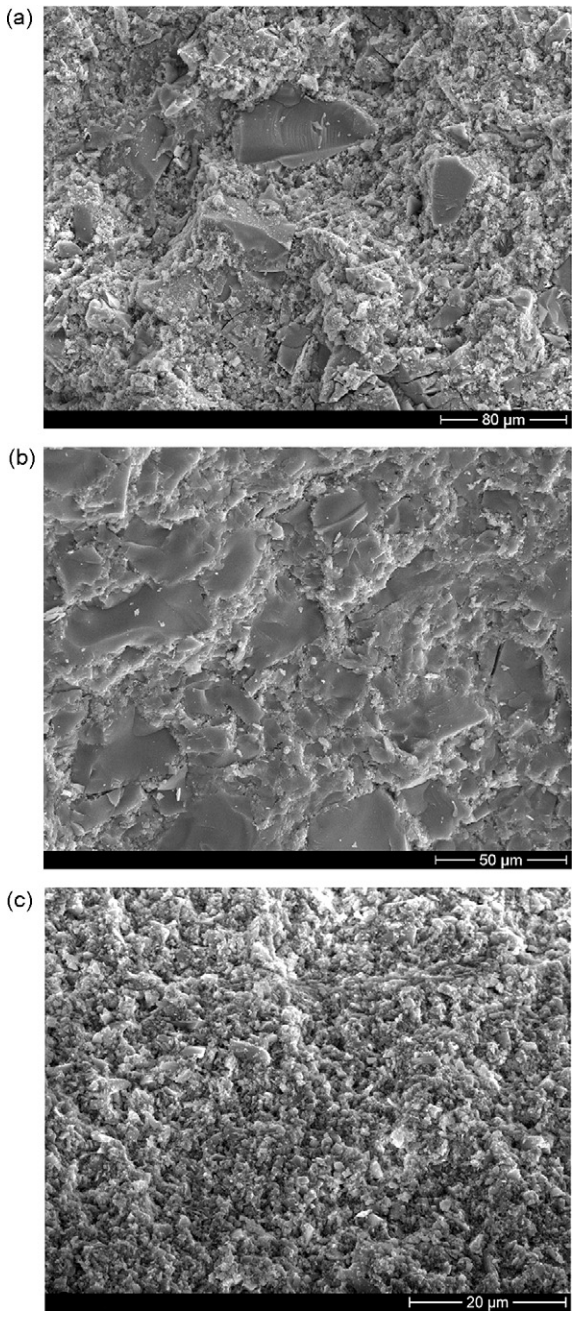

Fig. 7. SEM images of green pellet microstructure of $8CeO_2$–8YSZ powder after attrition grinding and pressing (a) at 190 MPa, (b) at 570 MPa and (c) powder after fractionation and pressing at 500 MPa.

To compare the compressibility curves of the powders synthesized by different methods, the parameter $\alpha = A_3/A_2$ may be used. This parameter characterizes the relative increase in the "compressibility" of powders in the region of high pressure (Table 1). For example, for our powders and for the powder Y-TZP N1[22] synthesized by a similar method (co-precipitation with washing in water and calcination), the values of $\alpha = A_3/A_2$ are in close agreement and equal 2.10 and 2.19, respectively. Using water for the washing of powders results in the formation

of strong agglomerates.[17,22] The mechanism behind agglomerate formation and possible cohesive forces between particles during synthesis and calcination were studied in detail in Ref. [24]. Using ethanol or isopropanol as a solvent (Y-TZP N3 and Y-TZP N4, respectively[22]) and Menhaden fish oil as a dispersant (Y-TZP N2[22]), the weak agglomerates were synthesized. In both cases, the powders were characterized by low values of α equal to 1.76, 1.47 and 1.64, respectively. Furthermore, the values of $P_{Y2} \sim 200$–250 MPa for these powders are significantly lower than those for our powders ($P_{Y2} \sim 573$ MPa) and for Y-TZP N1 ($P_{Y2} \sim 392$ MPa) synthesized using water as a solvent.

Thus, on the basis of our results and the model approximations proposed in Refs. [10,16], we can assume that the presence of a second break on the compressibility curves could arise as a result of the fragmentation of strong aggregates up to the primary crystallites. The value of P_{Y2} denotes the average compressive strength of the aggregates. The strength of the aggregates is determined by the packing type of the primary crystallites and the number of necks between the crystallites. The fragmentation of aggregates occurs by breaking of the necks. This process was particularly investigated in Ref. [10].

The morphological structures of the green bodies were investigated by SEM. For the powder after drying, representative SEM images of pellets pressed at 190 MPa ($P < P_{Y2}$) and at 570 MPa ($P > P_{Y2}$) are shown in Fig. 7a and b, respectively. As was described above, the "hard" agglomerates consist of the high packing primary particles; therefore the contribution of these agglomerates to the powder densification is insignificant. During of compression, the cracking and repacking of the "hard" agglomerates only take place, Fig. 7a and b. The increasing green body density occurs mainly as a result of the densification of the "soft" agglomerates. This is evident from a significant decrease in the thickness of the "soft" agglomerates layer located between the coarse "hard" agglomerates as the compaction pressure increases, Fig. 7a and b, respectively. For the pellet pressed at 190 MPa ($P < P_{Y2}$), the place between "hard" agglomerates is filled up the "soft" agglomerates with the low-packed density, Fig. 7a. With the increasing of compaction pressure, the distance between "hard" agglomerates decreases and the density of "soft" agglomerates placed between "hard" agglomerates increases, Fig. 7b.

3.2. Sinterability of the powders

After compaction, the pellets were sintered at 1600 °C for 5 h in air atmosphere. The sinterability of the powders after drying (110 °C) and after calcination at 350, 600 °C was investigated as a function of the compaction pressure.

The sinterability curves of the powders after drying at 110 °C have a pronounced maximum in the region of small pressures (Fig. 8). If the optimal compaction pressure (P^*) corresponds to the pressure at the maximum value of sintered density, then P^* is located between 250 and 350 MPa. In this region, pellets reach densities of up to $\rho_S^* = 0.924$ TD. The pellets prepared from dried powders are sensitive to under- and over-pressing. The low values of the green densities and the material crystallization

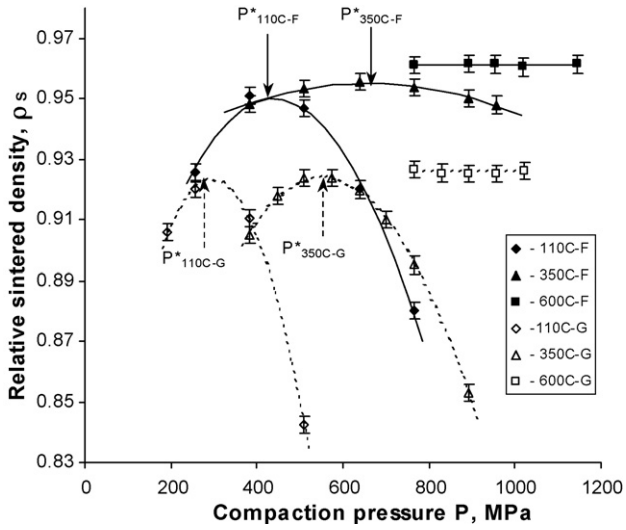

Fig. 8. Relative sintered density of $8CeO_2$–8YSZ pellets made from ground (open symbols) or fractionated (full symbols) powder, as a function of compaction pressure and calcination temperature.

accompanied by the elimination of a considerable amount of water from the samples are responsible for these sensitivities.

The sinterability curve of the powders calcined at 350 °C also has a maximum but in the region between 500 and 600 MPa (Fig. 8). By increasing the calcination temperature, the optimal pressure region is enlarged and shifts to higher pressures. In the region of the optimal compaction pressure, pellets also reach densities of up to 0.92–0.93.

The sinterability of powders calcined at 600 °C has no pressure dependence at high pressures (Fig. 8). In the pressure range from 600 to 1000 MPa, the densities of the sintered pellets are constant and the samples have similar physical properties. Pressures higher than 750 MPa can, therefore, be chosen as optimal compaction pressures. In the case of the powder calcined at 600 °C, pellets reach densities of up to 0.926.

Thus, by increasing the calcination temperature, the optimal pressure increases, and the region of optimal pressure are enlarged. The values of the optimal compaction pressures (P^*) and corresponding sintered densities (ρ_S^*) are summarized in Table 2.

As is obvious from the comparison of the values shown in Tables 1 and 2, the optimal pressure (P^*) is always smaller than the pressure of the secondary breakpoint (P_{Y2}). For all investigated powders, the region of optimal pressures is located in the upper part of the middle-pressure region, whereas the

Table 2
Optimal compaction pressures (P^*) and sintered densities (ρ_S^*).

T_C (°C)	Treatment	P^* (MPa)	ρ_S^*
110	G	300	0.924
350	G	530	0.924
600	G	750	0.926
110	F	430	0.95
350	F	650	0.955
600	F	760	0.961

G, ground; F, fractionated.

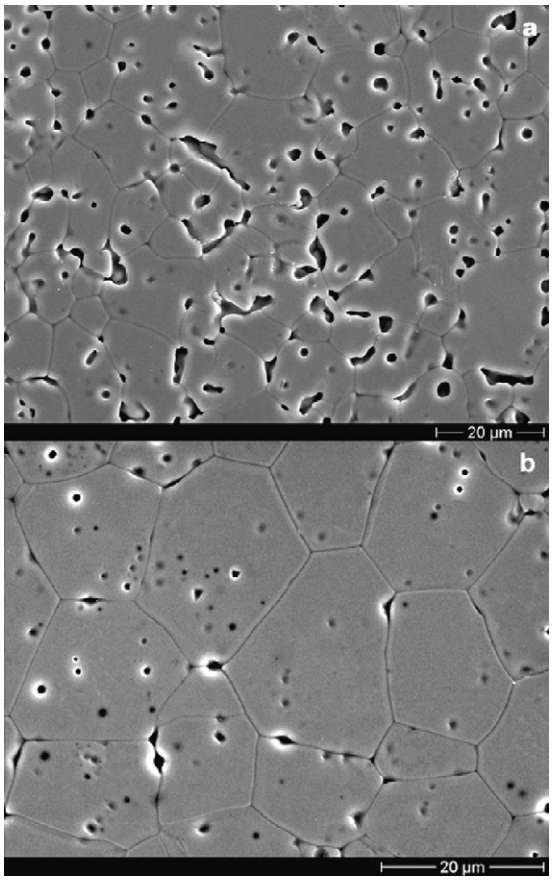

Fig. 9. SEM images of pellets sintered from (a) ground and (b) fractionated powders.

P^*/P_{Y2} ratio varies from 0.7 to 0.9. For all investigated powders, the region of the optimal pressures is illustrated in Fig. 6 by the big dotted square. As was assumed earlier, at pressure P_{Y2} and higher, fragmentation of the strong aggregates up to the primary crystallites disturbs the contact between the primary particles (neck). The deterioration of the contact between primary particles may in turn result in the deterioration of the sinterability.

The peculiarity of the sintering of the "soft" and "hard" agglomerates and the influence of this on the microstructure of the sintered pellets was investigated in detail in Ref. [25]. It was shown that the coarse "hard" agglomerates control the sintering to a large degree. They form a "rigid" skeletal during sintering and lead to the formation of extended pores along the grain boundaries.

The pellets prepared at optimal compaction pressure and sintered at 1600 °C were investigated by SEM (Fig. 9a). The sintered material is characterized by well-formed grains and grain boundaries, as well as by homogeneously distributed pores, which are mainly located at triple grain boundary junctions and inside the grains (Fig. 9a). The spherical pores are large and the average size is in the order of 2 μm. The extension of the pores located along the grain boundaries amounts to 20 μm.

Though the sintered pellets have a relatively low density (0.92–0.93 TD), they were produced using a simple wet technique (synthesis – drying or low temperature calcination – soft, dry attrition grinding – sintering), which can be adapted for the processing of radiotoxic materials. As was described in Refs. [26,27], the ceramic for the inert matrix fuel must have a relatively low density (~0.9 TD) and a well-formed microstructure and porosity.

The possibility of increasing the density of the sintered ceramic by using powders after fractionation by sedimentation in acetone was partially investigated in Ref. [25]. The morphological structure of green bodies produced from the powder after fractionation is very uniform and contains mainly "soft" agglomerates (Fig. 7c).

After sintering the pellets are characterized by a homogeneous morphological structure. They have well-formed grains and grain boundaries and uniformly distributed pores (Fig. 9b). Moreover, the absence of coarse "hard" agglomerates in the powder leads to the absence of large pores in the sintered material. The pores are small with an average size of 0.5–0.8 μm and they are located mainly within the grains.

The sinterability of the pellets prepared from fractionated powders was also investigated in detail as a function of the compaction pressure (Fig. 8). Similar to the case of the ground powders, pellets prepared from fractionated powders and calcined at 110 or 350 °C are sensitive to under- and over-pressing. However, the region of the optimal compaction pressure (P^*) is extended and shifts to a higher pressure. Thus, for the fractionated powder ($T_C = 110$ °C), the optimal pressure region is located between 350 and 550 MPa reaching densities of up to 0.95 TD. Powders calcined at 350 °C have an optimal pressure region between 500 and 800 MPa reaching densities of up to 0.955 TD. Powders calcined at 600 °C have no pressure dependence at high pressure and reach values of 0.960 TD. For all powders, the fractionation led to an increase in density (Fig. 8 and Table 2).

The sintered pellets have a high density (0.95–0.96 TD) and well-formed microstructure. They were also produced by a simple wet technology, which can be easily adapted for the processing of radiotoxic materials. This ceramic may be used as an inert matrix for the final disposal of nuclear waste.[9]

4. Conclusion

In the present work, CeO_2–8YSZ powders containing between 8 and 12 mol% ceria were prepared by employing a co-precipitation method. After calcination at different temperatures and after mild attrition grinding, the compressibility and sinterability of the powders were investigated.

The compressibility curves were characterized by three linear regions at low, middle and high pressures. The middle and high regions of the compaction pressure, as least investigated, were studied in detail. The specific values of the compaction pressure (P_{Y2}) and density (ρ_{Y2}) at the intersection point of the compressibility curve were determined for all investigated powders.

It was shown that the compressibility curves for the $8CeO_2$–8YSZ powders after calcination at 110, 350, 600 °C and for the $12CeO_2$–8YSZ powder after drying in special coordinates ρ_G/ρ_{Y2} and $\log(P/P_{Y2})$ can be described by two straight

lines:

$$\frac{\rho_G}{\rho_{Y2}} = 1 + 0.23 \ \log\left(\frac{P}{P_{Y2}}\right) \quad \text{for} \quad P < P_{Y2}$$

$$\frac{\rho_G}{\rho_{Y2}} = 1 + 0.56 \ \log\left(\frac{P}{P_{Y2}}\right) \quad \text{for} \quad P > P_{Y2}$$

The empirical coefficients equal to 0.23 and 0.56 are universal parameters of the "compressibility" of a powder, which is mainly determined by the method of powder synthesis used.

It was assumed that the presence of the second break in the compressibility curves was due to the fragmentation of strong aggregates up to the primary crystallites. The value of P_{Y2} denotes the average compression strength of the aggregates.

The sinterability curves of powders after drying and after calcination at 350 °C had a pronounced maximum. The sinterability of powders calcined at 600 °C had no pressure dependence in the investigated pressure region. The optimal compaction pressures (P^*) corresponding to the pressure at the maximal value of the sintered density were determined for all investigated powders. It was shown that the region of optimal pressure is located in the upper part of the middle-pressure region, whereas the P^*/P_{Y2} ratio varies from 0.7 to 0.9.

The influence of powder fractionation on the sinterability of the powders was studied in detail as a function of the compaction pressure and calcination temperature. The microstructure of the pellets prepared at optimal compaction pressure and sintered at 1600 °C was investigated.

Acknowledgement

This work was supported by the European Union (EUROPART, contract no. F16W-CT-2003-508854).

References

1. Heimann, R. B. and Vandergraaf, T. T., Cubic zirconia as a candidate waste form for actinides: dissolution studies. *J. Mater. Sci. Lett.*, 1988, **7**, 583–586.
2. Matzke, H., Rondinella, V. V. and Wiss, T., Materials research on inert matrices: a screening study. *J. Nucl. Mater.*, 1999, **274**, 47–53.
3. Ledergerber, G., Degueldre, C., Heimgartner, P., Pouchon, M. A. and Kasemeyer, U., Inert matrix for the utilisation of plutonium. *Prog. Nucl. Energy*, 2001, **38**(3–4), 301–308.
4. Oversby, V. M., McPheetes, C. C., Degueldre, C. and Paratte, J. M., Control of civilian plutonium inventories using burning in a non-fertile fuel. *J. Nucl. Mater.*, 1997, **245**, 17–26.
5. Gong, W. L., Lutze, W. and Ewing, R. C., Zirconia ceramics for excess weapons plutonium waste. *J. Nucl. Mater.*, 2000, **227**, 239–249.
6. Fernandez, A., Haas, D., Konings, R. J. M. and Somers, J., Transmutation of actinides. *J. Am. Ceram. Soc.*, 2002, **85**(3), 694–696.
7. Dean, J. A., *Lange's Handbook of Chemistry* (*14th edition*). McGraw-Hill, New York, 1992.
8. Pepin, J. G. and McMarthy, G. J., Phase relation in crystalline ceramic nuclear waste form: the system UO_{2+x}–CeO_2–ZrO_2–ThO_2 at 1200 °C in air. *J. Am. Ceram. Soc.*, 1981, **64**(9), 511–516.
9. Degueldre, C. and Paratte, J. M., Concept for an inert matrix fuel, an overview. *J. Nucl. Mater.*, 1999, **274**, 1–6.
10. Dodd, A. C. and McCornick, P. G., Synthesis and processing of ultrafine Mg–PSZ powder. *J. Metastable Nanocrystall. Mater.*, 1999, **312–314**, 221–226.
11. Lange, F. F., Sinterability of agglomerated powders. *J. Am. Ceram. Soc.*, 1984, **67**(2), 83–89.
12. Fayer, M. E. and Otten, L., *Handbook of Powder Science and Technology* (*2nd edition*). Chapman&Hall, New York, 1977, p. 635–82.
13. Kouzov, P. A., *Basis for Analysis of Industrial Dust and Ground Materials Dispersion*. Khimia, Leningrad, 1974, p. 280.
14. Kawakita, K. and Ludde, K. H., Some considerations on powder compression equations. *Powder Technol.*, 1970/1971, **4**, 61–68.
15. Groot Zevert, W. F. M., Winnubst, A. J. A., Theunissen, A. J. A. and Burggraaf, A. J., Powder preparation and compaction behaviour of fine-grained Y-TZP. *J. Mater. Sci.*, 1990, **25**, 3449–3455.
16. Jorand, Y., Taha, M., Missiaen, J. M. and Montanaro, L., Compaction and sintering behavior of sol–gel powders. *J. Eur. Ceram. Soc.*, 1995, **15**, 469–477.
17. Van de Graaf, M. A. C. G., Ter Maat, J. H. H. and Burggraaf, J. A., Microstructure and sintering kinetics of highly reactive ZrO_2–Y_2O_3 ceramics. *J. Mater. Sci.*, 1985, **20**, 135–138.
18. Youshaw, R. A. and Halloran, J. W., Compaction of spray-dried powders. *Ceram. Bull.*, 1982, **61**(2), 227–230.
19. Messing, G. L., Markhoff, C. J. and McCoy, L. G., Characterization of ceramic powder compaction. *Ceram. Bull.*, 1982, **61**(8), 857–860.
20. Lukasiewicz, S. J. and Reed, J. S., Character and compaction response of spray-dried agglomerates. *Ceram. Bull.*, 1978, **57**(9), 798–801.
21. Matsumoto, R. L. K., Analysis of powder compaction using a compaction rate diagram. *J. Am. Ceram. Soc.*, 1990, **73**(2), 465–468.
22. Hare'l, G., Ravi, B. G. and Chaim, R., Effects of solvent and agitation on microstructural characteristics of sol–gel derived nanocrystalline Y-TZP powders. *Mater. Lett.*, 1999, **39**, 63–68.
23. Li, J. and Ye, Y., Densification and grain growth of Al_2O_3 nanoceramics during pressureless sintering. *J. Am. Ceram. Soc.*, 2006, **89**(1), 139–143.
24. Kaliszewski, M. S. and Heuer, A. H., Alcohol interaction with zirconia powders. *J. Am. Ceram. Soc.*, 1990, **73**(6), 1504–1509.
25. Bukaemskiy, A. A., Barrier, D. and Modolo, G., Physical properties of 8 mol% Ceria doped yttria stabilised zirconia powder and ceramic and their behaviour during annealing and sintering. *J. Eur. Ceram. Soc.*, 2006, **26**, 1507–1515.
26. Lee, Y. W., Kim, H. S., Kim, S. H., Joung, C. Y., Na, S. H., Ledergerber, G. *et al.*, Preparation of simulated inert matrix fuel with different powders by dry milling method. *J. Nucl. Mater.*, 1999, **274**, 7–14.
27. Lee, Y. W., Kim, H. S., Kim, S. H., Joung, C. Y., Lee, S. C., Na, S. H. *et al.*, Measurement of the mechanical properties of thermally-shocked zirconia-based simulated inert matrix fuel. *Prog. Nucl. Energy*, 2001, **38**(3–4), 231–236.